Engineering Structures 305 (2024) 117623

Contents lists available at ScienceDirect

Engineering Structures

journal homepage: www.elsevier.com/locate/engstruct

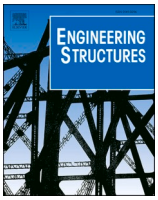

# Assessment of alternative design approaches for seismic upgrading of RC frame structures with steel exoskeletons

Francesco Nigro [a], Gaetano Della Corte [b], Enzo Martinelli [a,*]

[a] University of Salerno, Dept. of Civil Engineering, via Giovanni Paolo II n.132, 84084 Fisciano, SA, Italy
[b] University of Naples Federico II, Dept. of Structures for Engineering and Architecture, Via Claudio 21, 80125 Napoli, NA, Italy

ARTICLE INFO

*Keywords:*
RC structures
Seismic upgrading
Steel bracing
FRP strengthening
Sustainability

ABSTRACT

The use of external steel bracing systems (named exoskeletons) has recently emerged as a convenient technique for seismic upgrading of existing RC structures, as it possibly limits disturbance or interruption of building occupancy. However, although some conceptual formulations of the design problem can be found in the scientific literature, there are no universally accepted design criteria. The present paper highlights how alternative design choices can reverberate their effects on (i) the seismic performance of the upgraded structural system, (ii) its economic and ecological impact. For the sake of simplicity and consistency with the most common approach of practicing engineers, the present study adopted a force-based seismic design approach. The critical discussion proposed herein was obtained by varying the intensity of the seismic base shear force adopted for the exoskeleton design. Results of the design assessment show that the adoption of larger values of exoskeleton seismic design forces may not be the most suitable choice, especially if economic and ecological impacts are taken into account.

## 1. Introduction

According to a recent report by the European Environmental Agency, Europe exhibits the highest proportion of land use among all continents worldwide [1]. In addition, policymakers are actively promoting the refurbishment and reuse of older constructions instead of their demolition and reconstruction. Furthermore, recent assessments conducted by the Italian society of engineers have indicated that substantial investments are required to improve the safety of the numerous existing buildings in Italy, due to the fact that merely 2% of these structures were constructed after the year 2000, when more stringent technical standards were introduced [2].

In order to tackle this matter, several experimental campaigns have been conducted over the past few decades to evaluate the efficacy of different kinds of intervention techniques, leading to the development of the *fib* bulletin 24 [3]. The bulletin categorizes structural interventions into two main classes: on one side, "member-level" techniques aim to improve capacity in deficient members, while, on the other side, "structure-level" techniques are intended to reduce demand on the existing structure.

With regard to the structure-level techniques, among the various possibilities, the use of additional bracing systems is usually regarded as a suitable choice for structures exhibiting insufficient lateral stiffness and/or resistance. New braces can be placed either internally i.e., inside the existing reinforced concrete (RC) frames, as "endoskeleton" [4], or externally as an entirely new steel frame referred to as "exoskeleton". In either case, multiple options are available for the bracing system, i.e. traditional vs. advanced bracing systems [5–10]. It is worth noting that a steel exoskeleton can be financially advantageous when there is a need to simultaneously enhance the energy efficiency of the building and when occupancy disruption should be avoided. However, it may be considered a viable solution only in cases where the building is located at sufficient distance from other structures [11–14]. Furthermore, in the field of energy and seismic upgrading of existing structures, it is possible to find in literature some explicative case studies related to this topic, taking into account the influence of infill walls as well [15,16].

Although numerous authors have addressed the conceptualization of the seismic retrofit problem [17], also regarding it as an optimization problem [18], it is worth noting that most of the currently available seismic design codes do not offer explicit design guidelines for a hybrid structure consisting of a reinforced concrete (RC) frame and a steel concentrically braced frame. One of the potential reasons for the lack of general design criteria in modern codes, as well as in the scientific literature, may be the large number of design variables, resulting in the

* Corresponding author.
*E-mail address:* e.martinelli@unisa.it (E. Martinelli).

https://doi.org/10.1016/j.engstruct.2024.117623
Received 9 October 2023; Received in revised form 14 January 2024; Accepted 4 February 2024
Available online 26 February 2024

difficulty to find a generally applicable solution. One relevant issue arising from preceding studies is the frequent need for a combination of local (i.e., member-level) and global (i.e., frame-level) interventions to reach modern code upgrading requirements [19]. Among the member level techniques, the use of FRP strengthening methods [20–23] is certainly an internationally recognized advantageous approach. Moreover, another relevant issue usually arising in the case of existing structures is the commonly adopted assumption of floors behaving as rigid diaphragms. Especially, when adopting steel exoskeletons located only at the perimeter of the building, this assumption might be questionable and should deserve research investigations [24,25].

To capture properly the efficiency of such upgrading interventions, it is in fact mandatory to model accurately the nonlinear behaviour of the existing structure equipped with exoskeletons. For instance, if a traditional concentrically braced frame (CBF) is selected, a proper nonlinear model of brace elements and their connections should be considered for structural design and analysis, as buckling and post-buckling phenomena can have adverse effects on the overall performance of the enhanced structure [26]. Besides, it might be suitable to perform nonlinear static (pushover) analyses, that are frequently employed for simulating the seismic response of structures, as they require neither accelerometric signals nor cyclic stress-strain relationships and it is sufficiently accurate to predict the overall response if higher vibration modes do not affect significantly the response [27–30].

The purpose of this study is to provide an overview of the multifarious aspects that can influence the practitioner decision-making process, with respect to design choices and seismic performance parameters, as well as taking into consideration the economic cost and environmental impacts of the interventions. To this aim, Section 2 describes the design methodology utilized for all the upgrading interventions, Section 3 provides relevant details about the modelling and assessment criteria utilized for both the existing and new structures, Section 4 presents a general description of an archetype existing structure to be upgraded. Lastly, Section 5 reports the most relevant results obtained through a pushover-based assessment of the upgraded structures, considering also their economic and ecological costs, whereas Section 6 summarizes the outcomes of the work with some conclusive remarks.

## 2. Design of the upgrading interventions

The current section illustrates the design criteria adopted for the upgrading interventions, including the new steel CBF exoskeletons, as well as the additional required interventions at member and foundation level.

First, the criteria to evaluate the design base shear forces for the CBFs are presented. Subsequently, a detailed description of the criteria adopted to evaluate internal forces acting on braces, beams and columns of the CBF system is provided. Eventually, the criteria to design the additional interventions, such as local-level strengthening with FRP and foundation design for the new steel exoskeleton, are described.

### 2.1. Design criteria for steel exoskeletons

#### 2.1.1. Design values of the base shear forces

As outlined in the introductory section of this paper, the current seismic design codes do not provide explicit design rules for the hybrid structural system comprising an older existing RC frame (usually with insufficient seismic resistance and lacking seismic details) and a new steel exoskeleton. Although a displacement-based approach is a logical and more straightforward option for designing such upgrading interventions, it requires quite a specialistic knowledge of the analysis methodologies. This specialization might be the reason why the spreading of a displacement-based approach among practitioners appears still limited. Therefore, the more commonly adopted force-based approach was selected for the present study.

This study investigates the effect of the design shear force of the exoskeleton on the resulting performance of the upgraded RC frame. Therefore, three design scenarios were explored. In a first scenario, it was assumed that the CBFs are the sole structural system resisting seismic forces. In other words, it was assumed that the designer would calculate the total base shear force of the system comprising both the older building and the new steel structure, while designing the new steel structure to resist this entire value of the lateral force. Instead, in a second and third scenarios, the intensity of the base shear force utilized to design the CBFs was obtained by multiplying the base shear force, determined as for the first scenario, by factors assumed equal to 0.75 and 0.50 respectively. This approach allowed to modulate the stiffness and resistance of the new steel structure relative to the existing RC frame structure.

The starting point of the design was the elastic design spectra given by the Italian technical code for the considered construction site [31]. Consequently, in the case of "Scenario 1", the exoskeletons were designed using the following equation, which is provided by Eurocode 8 [32]:

$$V_{\mathrm{bd,Scenario1}} = \left(\lambda m_{tot}\right)\cdot\delta\cdot\frac{S_a\left(T_{1,CBFs}, PGA_{SD}\right)}{q_{CBFs}} = \left(\lambda m_{tot}\right)\cdot\delta\cdot\frac{F_0\cdot\eta\cdot S\cdot PGA_{SD}}{q_{CBFs}} \quad (1)$$

In Eq. (1) the symbols have the following meaning:

- $\lambda$ (equal to 0.85 in the current application) accounts for the fact that in buildings with at least three storeys (and, no torsional effects) the effective modal mass of the fundamental mode is smaller than the total building mass, on average by 15%;
- $m_{tot}$ is the total mass of the structure in the seismic load combination;
- $\delta = 1.3$ is an amplification coefficient representing the effect of accidental torsional effects;
- $S_a(T_{1,CBFs}, PGA_{SD})$ is the Severe Damage (SD) limit state spectral ordinate corresponding to the fundamental period of the structure, which is estimated as $T_{1,CBFs} = 0.05{\cdot}H^{3/4}$ ($H$ being the height of the structure expressed in meters);
- $PGA_{SD}$ is the Peak Ground Acceleration for SD limit state;
- $q_{CBFs}$ is the behaviour factor, which is equal to 4 in case of CBFs;
- $F_0$ is a site amplification factor, equal to 2.29;
- $\eta$ is a damping factor, which was always assumed equal to unity for an equivalent elastic viscous damping ratio of 5%;
- $S$ considers the type of soil and is equal to 1.34 for the SD Limit State.

However, since there is no clear and generally accepted method to estimate the fundamental periods of the hybrid RC frame structures with steel bracing, the adoption of the maximum spectral ordinate is advantageous, because it allows for an easier parametric design and analysis of the upgrading interventions.

For the remaining two design scenarios, the design shear force obtained by means of Eq. (1) is reduced to account roughly for the contribution of the existing RC structure:

$$V_{\mathrm{bd,Scenario2}} = 0.75{\cdot}V_{\mathrm{bd,Scenario1}} \quad (2)$$

$$V_{\mathrm{bd,Scenario3}} = 0.50{\cdot}V_{\mathrm{bd,Scenario1}} \quad (3)$$

Therefore, in the present study Scenarios 1, 2 and 3 are also referred to as "F100", "F75" and "F50".

#### 2.1.2. Design of steel exoskeletons

In the following description, reference is made to an individual 2D braced frame with two separate diagonal brace members. It is assumed that the distribution of the total base shear force for the entire building among the individual braced bays has been carried out according to some simplified analysis of the plan distribution of the braced bays. The design value of the base shear force for the individual braced bay is indicated again by the symbol $V_{bd}$, to simplify the notation.

Once the base shear force on the individual braced bay was calcu-

lated, the distribution of the storey shear forces was assumed according to the well-known approximation shown by Eq. (4):

$$V^{(i)}{}_{Ed} = \frac{\sum_{j=i}^{n_{st}} z_j \cdot W_j}{\sum_{j=1}^{n_{st}} z_j \cdot W_j} \cdot V_{bd} \tag{4}$$

where $V_{Ed}^{(i)}$ is the i-th storey shear force, $z_j$ represents the height of the j-th storey with respect to the top of the foundation level, $W_j$ denotes the seismic weights of the j-th storey, $V_{bd}$ is the total base shear force for the design and $n_{st}$ is the number of storeys.

Subsequently, for each storey, the diagonal brace members were designed to withstand the equivalent static shear force while neglecting the contribution of braces in compression. The assumption to neglect compression braces follows the suggestion of the current Italian seismic code [31], which in turn reproduces the proposal of the former Eurocode 8 [32]. This choice was made to reproduce the typical practice followed by designers in the last few years in Italy. Consequently, the design value of the brace axial (tension) force $N_{br,d}^{(i)}$ was evaluated by means of Eq. (5):

$$N^{(i)}{}_{br,d} = \frac{V^{(i)}{}_{Ed}}{\cos(\alpha^{(i)}{}_{br})} \tag{5}$$

where $\alpha_{br}$ is the brace angle formed with the horizontal axis at the i-th storey and, $V_{Ed}^{(i)}$ the storey shear force derived from Eq. (4). In addition to the resistance check, the design of the diagonal braces is influenced by the code limitations onto the overstrength ratio $\Omega$. The overstrength ratio is defined as the ratio between the tension plastic resistance $N_{pl,Rd} = A \cdot f_{yk}/\gamma_{M0}$ (being $A$ the cross section area, $f_{yk}$ the characteristic value of steel yielding strength and $\gamma_{M0}$ a partial safety factor for tension resistance) and the corresponding axial force demand given by Eq. (5). In fact, indicating by $\Omega_{min}$ and $\Omega_{max}$ the minimum and maximum values of $\Omega$, the code stipulates satisfaction of the requirement shown by Eq. (6):

$$\frac{\Omega_{\max} - \Omega_{\min}}{\Omega_{\min}} \leq 0.25 \tag{6}$$

In addition, the code provides a limit value to the brace slenderness $\lambda$, which should satisfy Eq. (7):

$$\bar{\lambda} = \sqrt{\frac{N_{pl}}{N_{cr}}} = \frac{\lambda}{\pi}\sqrt{\frac{f_y}{E}} \leq 2.0 \tag{7}$$

where $N_{cr}$ is the Eulerian buckling load.

After selecting the diagonal brace cross sections, the design of beams and columns ("non-dissipative" members) was carried out. To this aim, a limit analysis approach was followed [33], considering the two limit conditions schematically represented in Fig. 1:

- the first design scheme adopted, depicted in Fig. 1(a), is based on the assumption that compression braces respond with their expected initial buckling axial force resistance, defined as $\chi \cdot N^{(i)}{}_{br,e,t} = \chi \cdot \gamma_{ov} \cdot \gamma_{M0} \cdot N^{(i)}{}_{br,pl,Rd}$, where $\gamma_{ov}$ is a material overstrength factor, $\gamma_{M0}$ is a partial safety factor for tension resistance and $\chi$ is the reduction factor due to flexural buckling. The current Italian seismic code stipulates $\gamma_{ov} = 1.25$, and $\gamma_{M0} = 1.05$;
- secondly, the structural scheme, as shown in Fig. 1(b), considering that tension braces develop their expected plastic resistance $N^{(i)}{}_{br,e,t} = \gamma_{ov} \cdot \gamma_{M0} \cdot N^{(i)}{}_{pl,Rd}$, whereas compression braces retain a residual post-buckling axial force capacity equal to 30% of the expected buckling (initial) capacity, $N^{(i)}{}_{br,res,c} = 0.3 \cdot N^{(i)}{}_{br,e,c} = 0.3 \cdot \chi \cdot N^{(i)}{}_{br,e,t}$ (with the same meaning as previously used symbols).

Indeed, recent analytical studies have demonstrated that CBFs conventionally designed using elastic design methods may experience significant damage or even structural failure when subjected to design level ground motions [34,35]. Moreover, it is worth noticing that the approach adopted for brace and beam-column sizing is consistent with research works relevant to this topic, assuming a global collapse mechanism of the structure and a post-buckling brace axial force proportional to the inter-storey drift, estimated through some simplified assumptions [36].

Thus, projecting the sum of the two aforementioned brace contributions onto the horizontal direction and applying the horizontal force equilibrium condition, the storey shear forces (and, subsequently the storey lateral forces) corresponding to the considered state (Fig. 1) of the braced frame can be evaluated as follows:

$$\lambda_b \cdot V_E^{(i)} = 2 \cdot \chi \cdot N^{(i)}{}_{br,e,t} \cdot \cos(\alpha^{(i)}{}_{br}) \tag{8}$$

$$\lambda_{pl} \cdot V_E^{(i)} = \left(N^{(i)}{}_{br,e,t} + N^{(i)}{}_{br,res,c}\right) \cdot \cos(\alpha^{(i)}{}_{br}) \tag{9}$$

$$\lambda \cdot F_E^{(i)} = \begin{cases} \lambda \cdot \left(V_E^{(i)} - V_E^{(i+1)}\right) & \text{if } i < n_{st} \\ \lambda \cdot V_E^{(i)} & \text{if } i = n_{st} \end{cases} \tag{10}$$

where, with reference to the i-th storey, $V_E$ and $F_E$ represent the shear force and horizontal force respectively, $\alpha_{br}$ is the brace angle onto the horizontal axis and, $\lambda_b$ and $\lambda_{pl}$ respectively represent the multipliers of the horizontal actions for the two schemes in Fig. 1(a) and Fig. 1(b) respectively.

Once such forces have been evaluated, it is possible to determine the

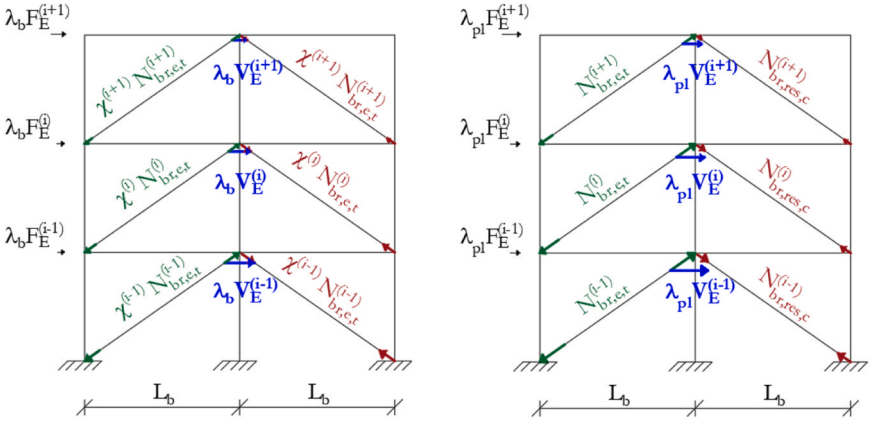


**Fig. 1.** Storey force evaluation.

design axial loads acting on both internal and external columns, as follows. For the scheme shown in Fig. 1(a) the axial load acting on the external columns is obtained by the following equations:

$$N^{(i)}{}_{Ed,col,ext,b} = \begin{cases} \sum_{j=i+1}^{n_{st}} \chi^{(j)} \cdot N^{(j)}{}_{br,e,t} \cdot \sin\left(\alpha^{(j)}{}_{br}\right) & \text{if } i < n_{st} \\ 0 & \text{if } i = n_{st} \end{cases} = \begin{cases} \frac{\lambda_b}{2} \sum_{j=i+1}^{n_{st}} V_E^{(i)} \cdot \tan\left(\alpha^{(j)}{}_{br}\right) & \text{if } i < n_{st} \\ 0 & \text{if } i = n_{st} \end{cases} \tag{11}$$

Conversely, for the scheme shown in Fig. 1(b), the axial load acting on the external columns are obtained using the following equations:

$$N^{(i)}{}_{Ed,col,ext,b} = \begin{cases} \sum_{j=i}^{n_{st}} N^{(j)}{}_{br,res,c} \cdot \sin\left(\alpha^{(j)}{}_{br}\right) & \text{for external columns in compression} \\ \sum_{j=i}^{n_{st}} N^{(j)}{}_{br,e,t} \cdot \sin\left(\alpha^{(j)}{}_{br}\right) & \text{for external columns in tension} \end{cases} \tag{12}$$

$$N^{(i)}{}_{Ed,col,\ int\ ,pl} = \sum_{j=i}^{n_{st}} \left(N^{(j)}{}_{br,e,t} - N^{(j)}{}_{br,res,c}\right) \cdot \sin\left(\alpha^{(j)}{}_{br}\right) \tag{13}$$

Finally, beam axial loads were evaluated, distributing the total story force to the three joints of the two braced bays and, subsequently distributing the force applied at the internal joint to the two adjacent beams:

$$N^{(i)}{}_{Ed,beam} = \frac{\lambda}{2} \cdot \left(V_E^{(i)} + \frac{F_E^{(i)}}{3}\right) \tag{14}$$

Adopting Eqs. (12–14), the cross sections of beams and columns can be selected by checking their strength and stability.

### 2.2. Additional interventions

As mentioned in the introduction, to obtain a complete picture of the upgrading process, it is fundamental to account also for any required upgrading interventions for the existing RC super-structure as well as at the foundation level.

#### 2.2.1. Local interventions on RC beam-column joints

Joint strengthening was considered, distinguishing external joints from internal joints. External joints were strengthened in shear by means of FRP quadriaxial textile layers, externally placed on the joint panel zone. This intervention gives rise to an increase of the joint shear resistance due to a horizontal action from a bonding force acting on the joint panel, thus reducing the maximum tensile stress to which it is subjected. In accordance with the *fib* bulletin 35 [20], the bonding force was taken equal to

$$F_h = A_f \cdot E_f \cdot \varepsilon_{fd} \tag{15}$$

where:

- $A_f$ is the equivalent FRP textile area (depending on the type of textile adopted);
- $E_f$ is the Young modulus;
- $\varepsilon_{fd}$ is the ultimate strain of the composite material.

As suggested by *fib* bulletin 35 [20], in the case of beam-column joints, the composite laminate is expected to exhibit debonding from the concrete surface when a strain equal to *0.4%* is reached. This approach is also consistent with an Italian research report discussing this topic [21].

Conversely, to include the required capacity enhancement for internal joints, their upgrading is fulfilled through concrete jacketing [37,38]. The effect of a 50 mm thick concrete jacket on beam-column joint capacity was taken into account during the post-processing stage.

Further details about the determination of the shear capacity of the upgraded joints is reported in Section 3.3.

#### 2.2.2. Foundation of the steel exoskeleton

Although the upgrading of foundation systems is often disregarded in similar papers, the present study takes into consideration this crucial aspect by figuring out the possibility of realizing an additional foundation system including cast-in-place self-drilling IRS (Repetitive Selective Injection) micro-piles.

A simplified, yet sufficiently general, design procedure was adopted with the aim to define the ultimate load capacity of the micro-piles, $Q_{lim}$, which results from the addition of the total resistance in correspondence to the pile tip, $P$, and the lateral (namely, skin) total resistance, $S$, being both related to the results of Standard Penetration Tests (SPT). Based on well-established practice [39], $P = 0.15\ S$ was assumed and, in the case of soils having layers with different mechanical properties, the skin resistance can be expressed as follows:

$$S = \sum_i \pi \cdot d_s{}^{(i)} \cdot L_s{}^{(i)} \cdot s^{(i)} = \pi \cdot d \cdot \sum_i \alpha^{(i)} \cdot L_s{}^{(i)} \cdot s^{(i)} \tag{16}$$

where:

- $d_s$ is the equivalent diameter (proportional to the perforation diameter $d$);
- $L_s$ is the length of the injected zone;
- $s$ is the unit tangential resistance at the interface between the injected zone and the surrounding soil, while $\alpha$ is an amplification coefficient; both s and $\alpha$ depend on the nature and the characteristics of the soil and the technology used and, they can be obtained from proper tables [39].

Eurocode 7 approach was followed with the aim to define design values of the relevant geotechnical properties [40]. Details about this aspect are omitted herein for the sake of brevity.

In the current application, a stratigraphic soil column, typical of the construction site, was considered. Table 1 resumes the soil features and the main assumptions made in the evaluation of the micro-pile load capacity.

On the morphologic side, to reduce the interaction between the existing and the new foundations, the two foundation layouts depicted in Fig. 2(a-b) were considered for any single steel column. The additional micro-pile at the centre of the foundation block in Fig. 2(b) was needed only for the F100 design scenario, while the foundation layout of Fig. 2(a) was adopted in the other cases. The required micro-pile length resulted equal to 16 m, 15 m and 11 m, for the F100, F75 and F50 design scenarios respectively.

## 3. Structural modelling

### 3.1. Existing RC structure

With the aim of performing nonlinear static (pushover) analyses, a

**Table 1**
Soil properties.

| Soil nature | Depth* (from – to) | α (-) | $N_{SPT}$ (-) | s (MPa) |
|---|---|---|---|---|
| Finely bedded silty sand | 0 – 6 m | 1,5 | 30 | 0.20 |
| Hard (overconsolidated) clay | 6 – 20 m | 1,1 | 40 | 0.27 |

* The depth is measured starting from the top surface of micro-piles.

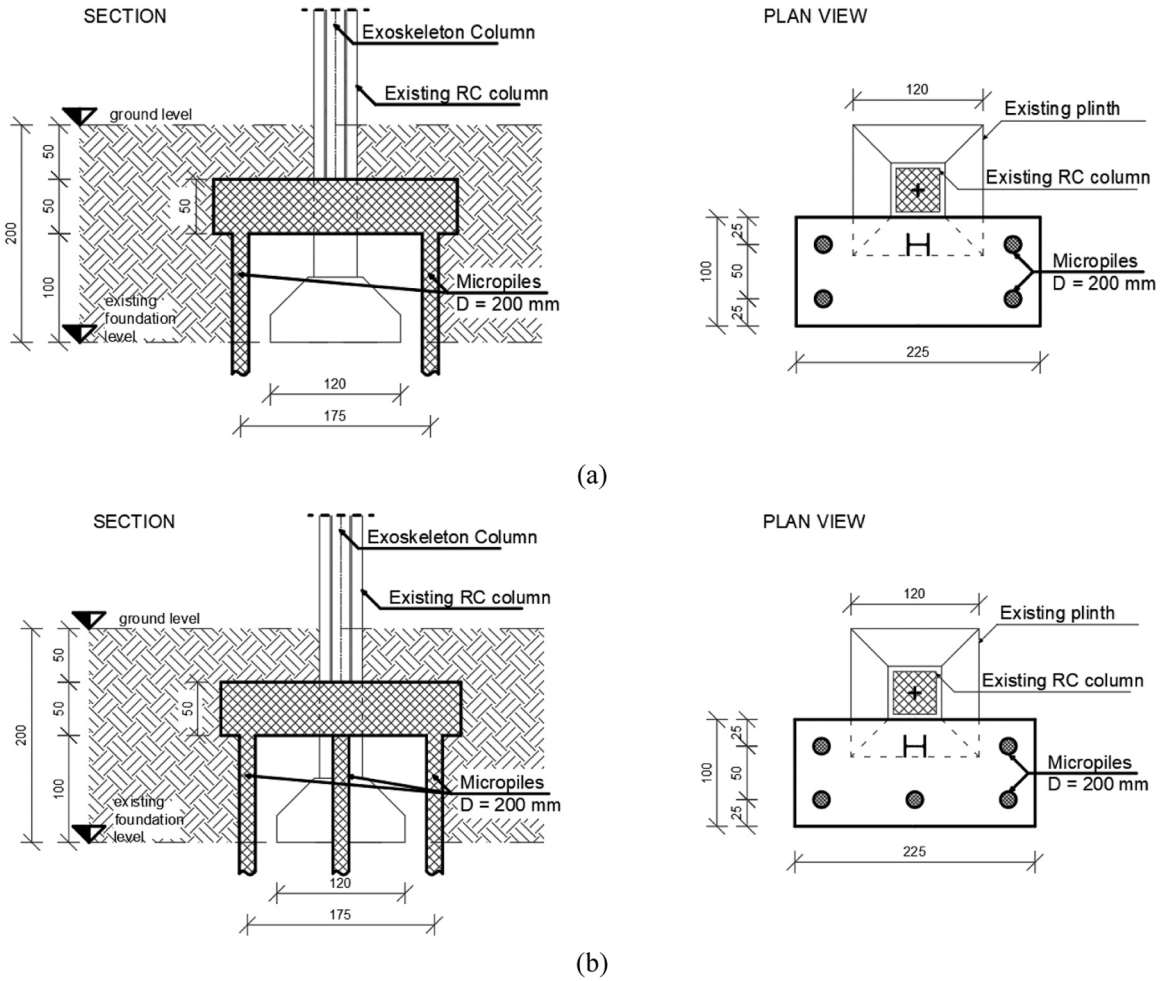


**Fig. 2.** Steel exoskeleton foundation layout.

nonlinear finite element (FE) model was developed using OpenSees [41].

Distributed plasticity elements were adopted for all RC members, accounting for both mechanical and geometrical non-linearities. Fiber sections were associated to each member, considering the uniaxial material models *Concrete01* and *Steel01* available in the OpenSees library. "Force-based" beam-column elements with 5 Gauss-Lobatto integration points were adopted. Brittle failures were not explicitly included in the FE model, but the shear capacity to demand ratios were evaluated in the post-processing phase, as outlined in a following part of the current section.

Expected material strengths were used for the analysis model. The average cylindrical compressive strength of concrete and yielding strength of the reinforcing bars were respectively assumed equal to $f_{cm}$ = 21 MPa and to $f_{sm}$ = 320 MPa, considered as the outcomes of in-situ tests on a structure representative of the assumed construction age (1960s).

For the sake of simplicity, floors were modelled as rigid diaphragms and the potential contribution of infilled frames was neglected.

### 3.2. Steel exoskeleton

#### 3.2.1. Braces

Braces were represented by means of force-based elements with a fiber discretization for their cross sections. Along their length, 4 sub-elements were used, each sub-element provided with 3 Gauss-Lobatto integration points. This mesh refinement was found sufficient to represent the buckling capacity by means of an equivalent geometric imperfection. A sinusoidal shape was assumed for the equivalent geometric imperfection, with a maximum imperfection amplitude $e_0$ assumed equal to 1/250 of the brace length, as suggested by Eurocode 3 for the case of a "Plastic Analysis" for CHS profiles belonging to the buckling curve "a" [42]. This approach was verified to provide a brace buckling capacity close to that obtained with the buckling curve.

On the contrary, beams and columns were modelled as straight elements (excluding geometrical imperfections) and using force-based fibre elements with 5 Gauss-Lobatto integration points. Finally, rigid end zones were considered at the ends of all members, based on the joint geometry reported in Section 3.2.2. Fig. 3 depicts the modelling choices discussed above.

#### 3.2.2. Steel connections

Joints between brace, beam and column converging into a node were modelled as shown in Fig. 4. To ensure in-plane buckling of the brace elements, the gusset plate and the brace were connected by a knife plate.

The brace end restraint condition can have a substantial impact on the structural capacity to resist buckling, tensile yielding, distribution of yielding, and post-buckling response of the dissipative components within the frame [43,44]. Therefore, a nonlinear rotational spring was introduced to represent the bending stiffness and capacity of the knife plate upon brace buckling. The spring rotational stiffness $k_{\phi,g}$ and moment resistance $M_{yg}$ were estimated on the basis of the geometric properties of the clearance provided at the brace ends, as depicted in Fig. 4, according to Eq. (17) and Eq. (18), respectively.

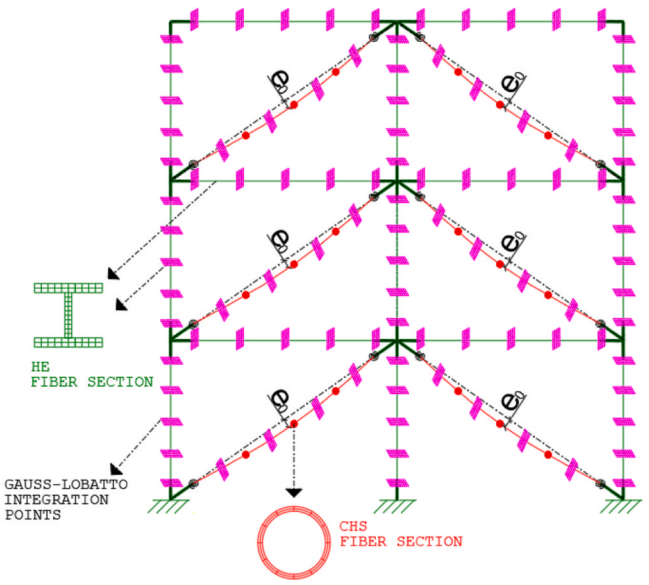


**Fig. 3.** Steel exoskeleton model.

$$k_{\varphi g} = 4 \cdot \frac{EI_g}{L_{gap}} = 4 \cdot \frac{E \cdot b_g \cdot t^3{}_g}{12 \cdot L_{gap}} \tag{17}$$

$$M_{yg} = f_{yk} \cdot W_g = f_{yk} \cdot \frac{b_g \cdot t^2{}_g}{4} \tag{18}$$

In the equations, $b_g$ and $t_g$ are the width and the thickness of the gusset plate, $L_{gap}$ is the length of the rotational clearance and $f_{yk}$ is the yielding strength of exoskeleton steel.

The remaining portion of the connection (involving beam and column ends, as well) was presumed to exhibit an almost rigid behaviour, due to the presence of the gusset plate, as evidenced by experimental studies concerning this topic [26]. Therefore, rigid end offsets were used, as shown in Fig. 4.

### 3.2.3. Connections between the existing RC structure and the steel exoskeleton

The connection between the new steel exoskeleton and the existing RC frame was not modelled explicitly, though some preliminary design was carried out to evaluate the construction costs (Section 5.2). For the numerical model, a kinematic constraint (*equalDOF* in OpenSees) was applied to the horizontal displacement components of the connected nodes in the two plan directions X and Y.

### 3.3. Criteria for seismic assessment of the existing and upgraded structures

To assess the performance of the existing RC structure, the capacity of RC members was evaluated at each analysis step, considering both ductile and brittle failure modes. With regards to the steel exoskeleton, cross section and buckling resistance of the steel beams and columns was checked.

The assessment of the existing RC structure was carried out according to the current Italian code [31], which is consistent with Eurocode 8 [45]. For the ductile failure modes, Damage Limitation (DL) and Severe Damage (SD) limit states were considered, conventionally corresponding to threshold values of the chord rotation reached in at least one of the primary seismic elements. More specifically, for the DL limit state a chord rotation capacity equal to 0.5% was adopted, to reduce the damage potentially occurring onto brittle non-structural elements attached to the structure (e.g. infill walls) and due to "frequent" earthquakes. Conversely, the chord rotation capacity for the SD limit state was evaluated for each RC column at each analysis step of the pushover analysis. The calculation procedure is detailed in Section 3.3.1. For the brittle failure modes, the SD limit state is associated with the shear strength capacity of RC members or beam-column joints. The mean values of material strengths, $f_{cm}$ and $f_{sm}$, were divided by some "confidence" factors for assessing the ductile failure modes, whilst for the brittle failure modes the expected material strengths were divided by the relevant partial safety factors. The confidence factors are used by the code to consider approximately the reliability of information available about the geometric and material properties of the existing structures. This reliability depends on the number and spread of surveys and material testing, which is in turn related to what the code defines as the "knowledge level". Assuming a "normal" knowledge level (labelled as KL2 by the code), the adopted confidence factor was $CF = 1.20$, whereas the partial safety factors were respectively equal to $\gamma_s = 1.15$ for steel and $\gamma_c = 1.50$ for concrete.

#### 3.3.1. Estimation of the chord rotation capacity at the SD limit state

For the SD limit state, the drift capacity of the RC columns was evaluated through the formulation provided by Eurocode 8 (Part 3, Section A.3.2.2) [45]. According to this formulation, in the case of existing structural elements, the "ultimate" drift capacity can be calculated as follows:

$$\vartheta_u = \frac{0.85}{\gamma_{el}} \cdot 0.016 \cdot 0.3^{\nu} \cdot \left[\frac{\max(0.01;\omega')}{\max(0.01;\omega)} \cdot f_c\right]^{0,225} \cdot \left(\frac{L_V}{h}\right)^{0,35} \tag{19}$$

where:

- 0.85 represents a coefficient introduced in the Italian Code [46] in the case of RC elements designed with no regard to modern seismic provisions;

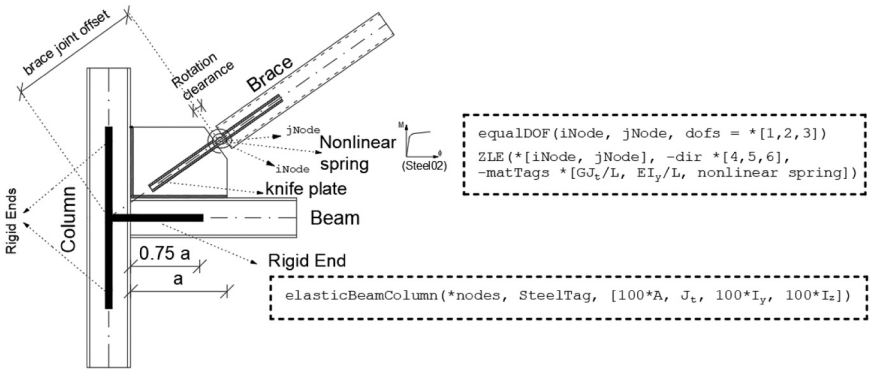


**Fig. 4.** Modelling of a brace and beam to column joint.

- $\gamma_{el}$ is a partial safety factor equal to 1.5 for primary seismic elements;
- $\nu$ is a normalized axial load, computed as $\nu = \frac{N}{b \cdot h \cdot f_c}$, being $N$ the external axial load, $b$ and $h$ the cross-section width and depth and $f_c$ the concrete compressive strength adopted in the case of ductile failure checks;
- $\omega = \frac{A_s \cdot f_s}{b \cdot h \cdot f_c}$ and $\omega' = \frac{A_s' \cdot f_s}{b \cdot h \cdot f_c}$ are the mechanical longitudinal reinforcement ratios, respectively for tension reinforcement ($A_s$, including also the reinforcement eventually placed along the beam web) and compression reinforcement ($A_s'$); $f_s$ is the steel yielding strength adopted for ductile failure checks;
- $L_V$ is the shear length of the member; it is assumed by the code to be equal to half of the element length.

According to the Eurocode provisions [45] (and Italian Code, as well [46]) the chord rotation capacity for the SD limit state is equal to *3/4* $\theta_u$.

### 3.3.2. Brittle mechanisms for RC members

Safety checks against brittle failures potentially occurring in RC members were performed for beams and columns, according to the Italian code, considering the variation of shear resistance with the chord rotation plastic demand. The Italian code utilizes the ratio between the plastic portion of the chord rotation demand and the chord rotation at yielding, $\mu_\Delta^{pl} = \frac{\theta_D - \theta_y}{\theta_y}$, to consider the effect of the inelastic deformations on the shear force resistance. Namely, the Italian provisions adopt the expression of the shear cyclic resistance (accounting for the resistance reduction under cyclic loading) provided by Eurocode 8 (Part 3, Section A.3.3.1) [45] when $\mu_\Delta^{pl} \geq 2$; conversely, when $\mu_\Delta^{pl} \leq 1$ the shear resistance is assumed equal to the maximum between the shear cyclic resistance and the shear resistance under monotonic loads as provided by Eurocode 2 [47]. For intermediate values of $\mu_\Delta^{pl}$ a linear interpolation is performed. For example, Fig. 5 shows the variation of the quantities involved in the resistance check of a column, highlighting the aforementioned quantities and the external shear action, as a function of the roof drift imposed with a pushover analysis.

For the beam-column joints, the safety check was performed by comparing the maximum tensile and compressive strengths (calculated by the application of the Mohr's circle method) with the tensile and compressive strength of unreinforced concrete joints, as shown by the following two equations:

$$\sigma_{jc} = \frac{N}{2A_j} + \sqrt{\left(\frac{N}{2A_j}\right)^2 + \left(\frac{V_j}{2A_j}\right)^2} \leq 0.5 f_{cd} \tag{20}$$

$$\sigma_{jt} = \left| \frac{N}{2A_j} - \sqrt{\left(\frac{N}{2A_j}\right)^2 + \left(\frac{V_j}{2A_j}\right)^2} \right| \leq 0.3\sqrt{f_{cd}} \tag{21}$$

where:

- $\sigma_{jc}$ and $\sigma_{jt}$ are the maximum compressive and tensile stresses;
- $f_{cd}$ is the concrete compressive strength assumed for brittle mechanisms;
- $A_j$ is the beam-to-column joint area evaluated as the product of $h_{jc}$ the distance between extreme layers of column reinforcement and the effective joint width $b_j$, defined in Eurocode 8 (Part 3, Section 5.5.3.3) [45];
- $N$ is the axial load acting on the column above the joint;
- $V_j$ is the joint shear demand (depending on the bending moments acting at the ends of the beams framing into the joint, as well as on the shear force acting on the column above the joint).

Furthermore, to evaluate the shear capacity $V_{jt}$ of external joints retrofitted with FRP textiles, as depicted in Section 2.2, Eq. (21) can be rewritten as follows:

$$V_{jt} = 0.3\sqrt{f_{cd}} \cdot A_j \cdot \sqrt{\left(1 + \frac{F_h}{0.3\sqrt{f_{cd}} \cdot A_j}\right) \cdot \left(1 + \frac{N}{0.3\sqrt{f_{cd}} \cdot A}\right)} \tag{22}$$

using the same symbols of Eq. (21) and deriving $F_h$ from Eq. (15). Conversely, the capacity enhancement required for internal joints is achieved through 50 mm thick concrete jacket, increasing the joint area $A_j$ reported in Eqs. (20)-(21).

### 3.3.3. Buckling resistance of steel beams and columns

Since the steel beams and columns were modelled using straight beam-column elements, the buckling resistance check of such members was performed step-by-step in the pushover analysis. To this aim, Eurocode 3 [42] was adopted to account for any potential buckling failure due to the simultaneous action of axial loads and bending moments.

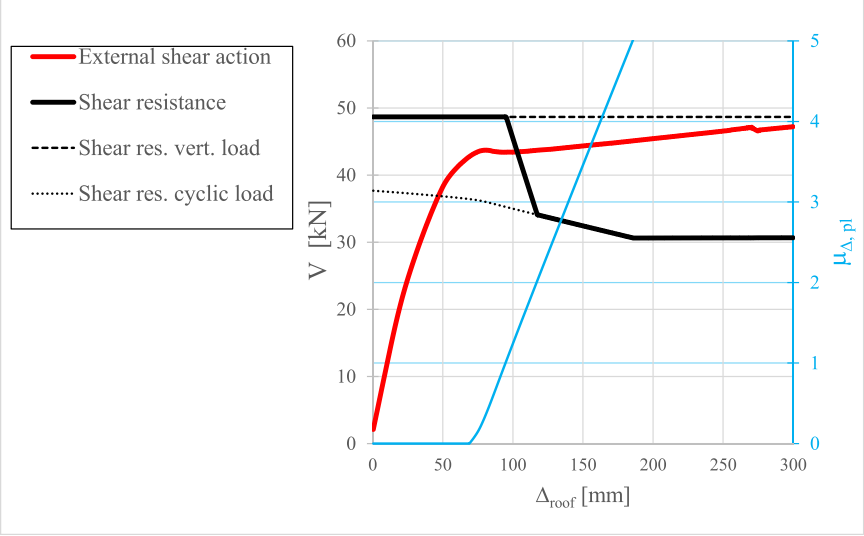


**Fig. 5.** Variation of a column shear force resistance with the chord rotation plastic demand $\mu_\Delta^{pl}$.

#### 3.3.4. Structural performance parameters

The following parameters were utilized to obtain a summarized description of the global seismic performance of the upgraded structure:

- The capacity-over-demand ratio in terms of Peak Ground Acceleration: $\zeta_E = \frac{PGA_C}{PGA_D}$;
- the Damage Extension Index $DEI = \frac{n_{LS}}{n_{tot}}$, accounting for the ratio between the number of structural elements failing the local resistance checks (unfavourable mechanisms) for each considered Limit State ($n_{LS}$) and the corresponding total number of structural elements $n_{tot}$.

## 4. Structure presentation

### 4.1. The archetype 1960s RC structure

An archetype 6-storey gravity load designed (GLD) structure was generated by simulating a design according to the Italian seismic code used in the 1960s [48]. The structure is characterized by 4 frames with 5 bays in the longitudinal (X) direction and 4 frames with 3 bays in the transversal direction (Y). Each bay has a length of 5.00 m, while the inter-storey height is constantly equal to 3.50 m. Considering the scope of this study, that is a proof of concept rather than a specific case study, the effect of the staircase was assumed to be negligible. Fig. 6 depicts the plan view of the structure and it also shows schematically the selected location of the steel exoskeletons.

The 1960s structural code was based on the allowable stress design method. With reference to typical materials used in the assumed construction age, the allowable stress was set equal to 8.5 MPa for concrete (*Rck25*) and 180 MPa for the reinforcing steel (*AQ60*).

Table 2 illustrates the loads adopted for the simulated design of the structure, while Table 3 and Table 4 summarize the design outcomes, in terms of column and beam cross sections respectively.

The assumed construction site (*Sant'Angelo dei Lombardi*, a small town in the South of Italy) is characterized by a high seismic hazard according to the current seismic zonation. Considering a soil class "C", as defined in the current Italian Seismic Code [31], for an earthquake return period of 475 years the design peak ground acceleration is $PGA_{SD}$=*0.266 g*, where the subscript "SD" refers to the so-called "severe-damage" limit state that is typically associated with that earthquake return period to form the performance objective. Similarly, considering an earthquake return period of 50 years for a "damage-limitation" limit state, the design peak ground acceleration is $PGA_{DL}$ = *0.082 g*. This information was used to design the upgrading interventions.

**Table 2**
Gravitational loads assumed for simulating the design of the structure.

| | | | |
|---|---|---|---|
| Floor | $G_{1k}$ | 3.00 | kN/m$^2$ |
| Permanent | $G_{2k}$ | 2.00 | kN/m$^2$ |
| Live | $Q_k$ | 2.00 | kN/m$^2$ |
| Infill walls | $g_{infill,k}$ | 7.00 | kN/m |

### 4.2. The prototype new steel exoskeletons

The estimated value of the fundamental vibration period of the steel CBF structure (determined as reported in Section 2.1) is equal to 0.49 s, corresponding to the plateau branch of the elastic design spectrum for SD Limit State. Consequently, the base shear forces assumed for the design of each single exoskeleton are equal to 1918 kN, 1438 kN and 959 kN, for the design scenario F100, F75 and F50 respectively. The cross sections correspondingly obtained for the CBF members, made of S 275 steel grade, are reported in Table 5. It is worth highlighting that column cross sections were selected to be constant at each storey, at least.

## 5. Comparative assessment of the upgraded structures

As previously outlined, the 3D models of the existing and upgraded structures were analyzed by means of non-linear static (pushover) analyses. Each pushover analysis was run up to a target displacement of 350 mm with a displacement increase of 0.50 mm per step. A height-wise linear distribution of horizontal forces was assumed. The N2-Method [29] was adopted to estimate the deformation and corresponding force demands.

In the following, the three upgrading scenarios are evaluated not only from the structural standpoint, but also comparing their cost

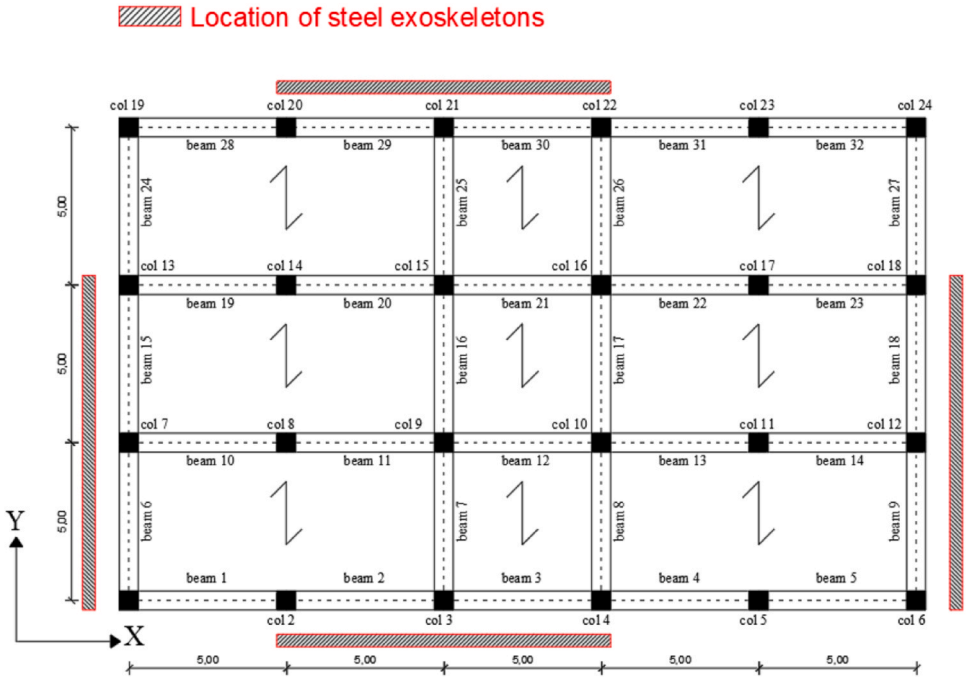


**Fig. 6.** Blueprint of the existing structure and location of the steel exoskeletons.

**Table 3**
Column cross sections and reinforcements.

| Storey | Column location | Cross section (cm x cm) | Longitudinal rebars | Stirrups |
|---|---|---|---|---|
| $6^{th}$ | corner | 30 × 30 | 4ϕ16 | ϕ8/25 cm |
| | border | 30 × 30 | 4ϕ16 | ϕ8/25 cm |
| | internal | 30 × 30 | 4ϕ16 | ϕ8/25 cm |
| $5^{th}$ | corner | 30 × 30 | 4ϕ16 | ϕ8/25 cm |
| | border | 30 × 30 | 4ϕ16 | ϕ8/25 cm |
| | internal | 30 × 30 | 4ϕ16 | ϕ8/25 cm |
| $4^{th}$ | corner | 30 × 30 | 4ϕ16 | ϕ8/25 cm |
| | border | 30 × 30 | 4ϕ16 | ϕ8/25 cm |
| | internal | 40 × 30 | 6ϕ16 | ϕ8/25 cm |
| $3^{rd}$ | corner | 30 × 30 | 4ϕ16 | ϕ8/25 cm |
| | border | 40 × 30 | 4ϕ16 | ϕ8/25 cm |
| | internal | 50 × 30 | 6ϕ16 | ϕ8/25 cm |
| $2^{nd}$ | corner | 40 × 30 | 4ϕ16 | ϕ8/25 cm |
| | border | 40 × 40 | 6ϕ16 | ϕ8/25 cm |
| | internal | 50 × 50 | 8ϕ16 | ϕ8/25 cm |
| $1^{st}$ | corner | 40 × 30 | 4ϕ16 | ϕ8/25 cm |
| | border | 40 × 40 | 6ϕ16 | ϕ8/25 cm |
| | internal | 50 × 50 | 8ϕ16 | ϕ8/25 cm |

effectiveness, considering both the initial cost and the life cycle cost.

It is worth highlighting that, following a code-compliant approach, the additional interventions at member and foundation level were designed in the "post-processing" phase, having performed the pushover analysis of the upgraded structures. This choice stems from the fact that the introduction of steel exoskeletons is able to modify the number and the location of members undergoing failure, as illustrated in Section 5.1.

### 5.1. Structural assessment

#### 5.1.1. Global seismic performance

The effect of the steel exoskeleton for each considered design scenario is reported herein in terms of pushover curves in the X and Y plan directions (Fig. 7 and Fig. 8, respectively). Specifically, Fig. 7(a) and Fig. 8(a) show results for the existing RC structure, while the subplots (b), (c) and (d) in Fig. 7 and Fig. 8 illustrate results obtained for the F50, F75 and F100 design scenarios, respectively. The plots in Fig. 7 and Fig. 8 highlight also the displacement capacity corresponding to each of the considered limit states. Eventually, the plots show also bilinear curves associated with the displacement capacity corresponding to a ductile failure mode. Such bilinear curves were obtained by equating the area under the curves, according to a procedure adopted by the Italian code [31], which requires the first branch of the bilinear curve to pass through the point of the pushover curve corresponding to 60% of its maximum base shear.

A comparison of performance among the various examined structures, in terms of the previously defined global safety index $\zeta_E$ for each relevant limit state, is instead reported in Fig. 9(a-b) that envelopes the results obtained respectively for the X and Y plan directions.

Comparing the results obtained for the bare RC frame and the RC structure equipped with the steel exoskeletons, it is apparent that the upgraded structures benefit from a significant increase in capacity for all the considered limit states, with the exception of the RC beam-column joints, which usually lack in ductility under lateral loading and fail in shear prior to the connected members.

With the latter exception, comparing the as-built and upgraded structures, the safety index $\zeta_E$ associated to all the limit states is generally more than doubled, thus resulting compliant with the safety requirement of modern seismic codes. Focusing on the variation of the global safety index with the changes in the design base shear force, Fig. 9 allows also to see that such relationship is nonlinear and sometimes even non monotonic.

Furthermore, the insertion of the steel exoskeletons did not modify significantly the magnitude of the roof displacement corresponding to ductile failure. However, the large increase in strength and stiffness characterizing the bilinear curves of the upgraded structures is able to reduce considerably the displacement demand, thus increasing appreciably the seismic intensity bringing damage to the RC structure. This

**Table 4**
Beam cross sections and reinforcements.

| Beam location | Cross section (cm x cm) | Top reinforcement | Mid reinforcement | Bottom reinforcement | Stirrups |
|---|---|---|---|---|---|
| Along X | 30 × 60 | 5ϕ16 | 2ϕ10 | 5ϕ16 | ϕ8/25 cm |
| Along Y | 30 × 40 | 3ϕ16 | 2ϕ10 | 3ϕ16 | ϕ8/25 cm |

**Table 5**
Cross sections of the steel exoskeleton members.

| Storey | F100 | | | F75 | | | F50 | | |
|---|---|---|---|---|---|---|---|---|---|
| | *Braces (CHS)* | *Columns (HE)* | *Beams (HE)* | *Braces (CHS)* | *Columns (HE)* | *Beams (HE)* | *Braces (CHS)* | *Columns (HE)* | *Beams (HE)* |
| $6^{th}$ | 168.3 × 4 | 340 B | 180 B | 139.7 × 4 | 300 B | 160 B | 114.3 × 3.2 | 240 B | 140 B |
| $5^{th}$ | 219.1 × 8 | 340 B | 180 B | 219.1 × 5 | 300 B | 160 B | 168.3 × 4.5 | 240 B | 140 B |
| $4^{th}$ | 219.1 × 10 | 340 B | 220 B | 219.1 × 8 | 300 B | 200 B | 219.1 × 5 | 240 B | 180 B |
| $3^{rd}$ | 219.1 × 12.5 | 340 B | 220 B | 219.1 × 10 | 300 B | 200 B | 219.1 × 6.3 | 240 B | 180 B |
| $2^{nd}$ | 219.1 × 16 | 340 M | 280 B | 219.1 × 12.5 | 300 M | 240 B | 219.1 × 7.1 | 240 M | 200 B |
| $1^{st}$ | 219.1 × 16 | 340 M | 280 B | 219.1 × 12.5 | 300 M | 240 B | 219.1 × 7.1 | 240 M | 200 B |

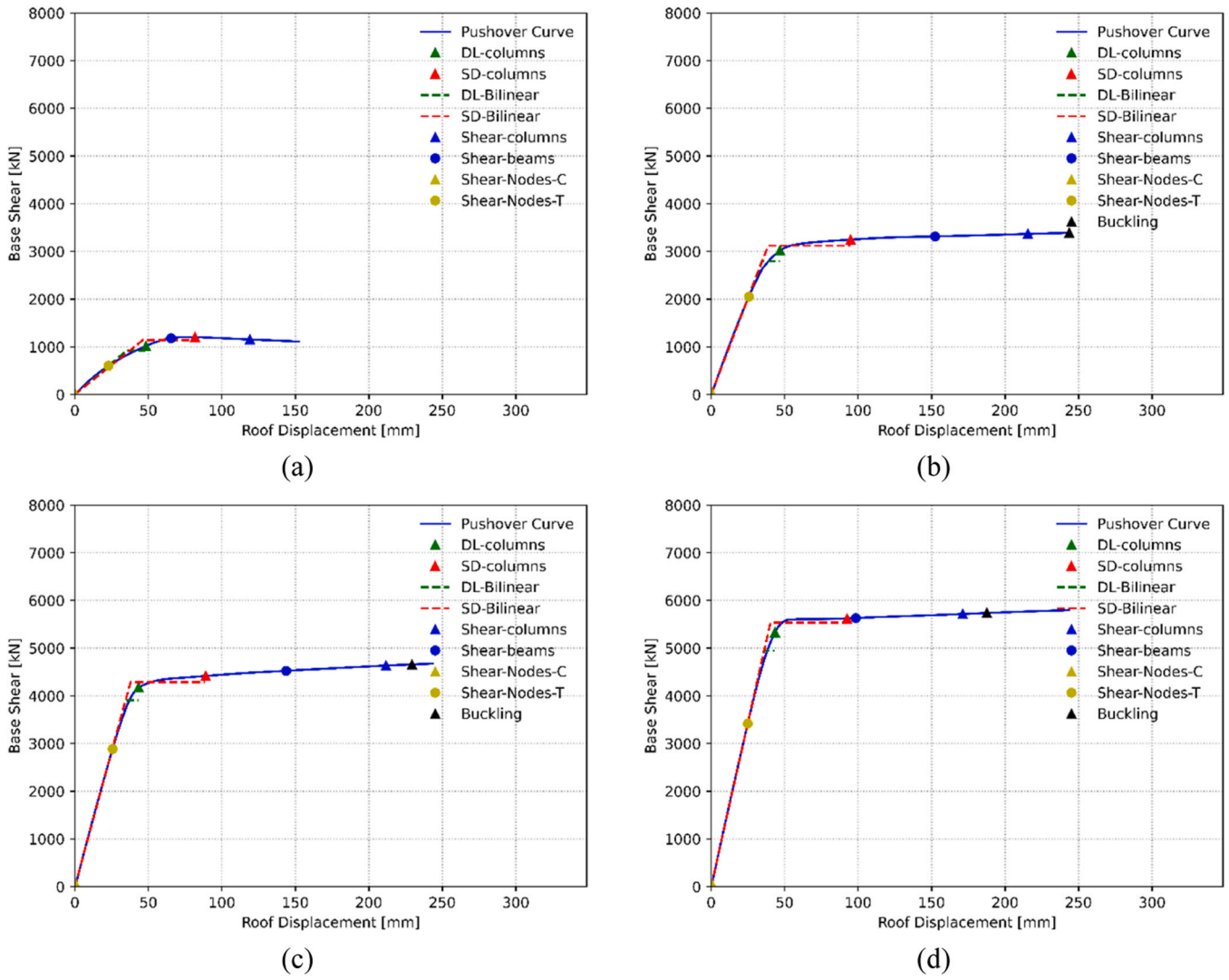


**Fig. 7.** SDOF X + Pushover curves and capacity points of the existing structure (a), F50 (b), F75 (c) and F100 (d) exoskeletons.

consideration is especially valid if the damage to the cladding and partitions is considered.

Eventually, it is worth mentioning that the displacement capacity corresponding to buckling of at least one non-dissipative member of the steel exoskeleton resulted always larger than the displacement capacity corresponding to other failure modes potentially occurring in the RC structure. Therefore, the results indicate the effectiveness of the design procedure reported in Section 2.1.

#### 5.1.2. *Spread of damage and failure mechanisms*

Focusing the attention on the damage potentially occurring onto the existing RC structure, despite the introduction of the steel exoskeletons, Fig. 10 reports the values of the DEI obtained for each failure mode. The results in Fig. 10 confirm that the "Joint Tensile" failure mode (Eq. (21)) is the only brittle failure mode that the steel exoskeletons were not able to delay significantly, even in the F100 design scenario (i.e., when the exoskeleton was designed totally neglecting the contribution of the existing RC frames).

With the exception of the RC beam-column joint shear failure, the results in Fig. 10 suggest that the steel exoskeletons were also able to significantly reduce the spread of damage, since the number of deficient members is always much smaller than it is in the bare RC frame.

However and unfortunately, the brittle shear failure mode of the beam-column joints represent the main weaknesses of the vast majority of existing RC structures. Fig. 11 compares for each different storey the number of joints undergoing shear failure. The plot refers to the push-over step corresponding to the estimated seismic deformation demand for the SD limit state. The results show that introducing the steel exoskeleton does not necessarily lead to a decrease of the failing joints at every storey. These results show also that some failures appear in the upgraded structures at storeys where the original bare RC frame did not show such failure. In fact, the steel exoskeleton modifies the distribution of the internal actions within the RC structure, resulting in the modification of the location of the failing joints.

### 5.2. *Intervention costs*

The initial intervention costs were estimated, taking into consideration all the processes involved in the making of the upgrading interventions, including the costs related to any demolition and restoration of the non-structural components of the existing RC building. Table 6 summarizes the unit costs associated to each intervention considered. Such costs were set with reference to the unit costs (for supply and installation) typical of the region where the structures are supposed to be located [49].

Fig. 12 summarizes the economic comparison among the

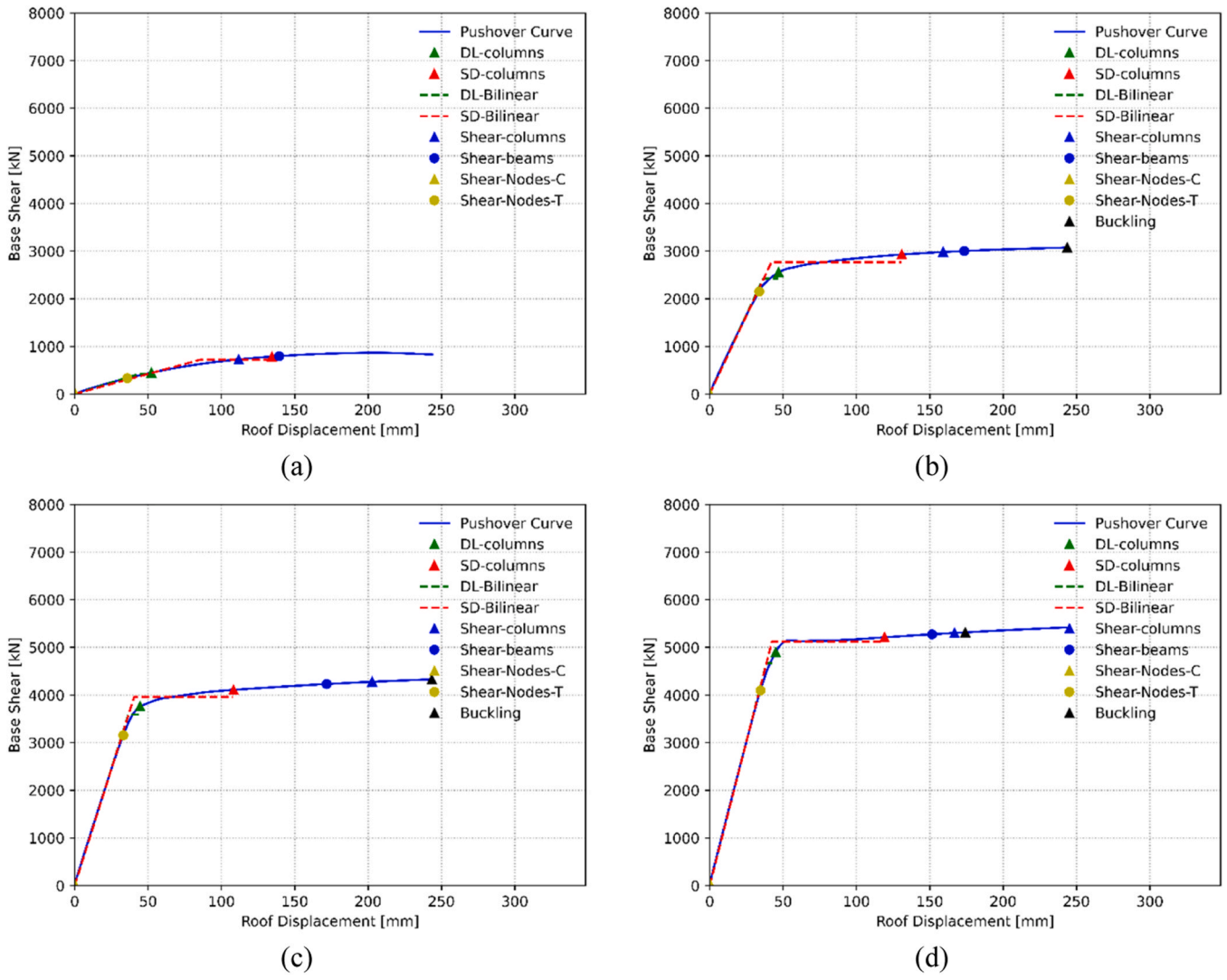


**Fig. 8.** SDOF Y+ Pushover curves and capacity points of the existing structure (a), F50 (b), F75 (c) and F100 (d) exoskeletons.

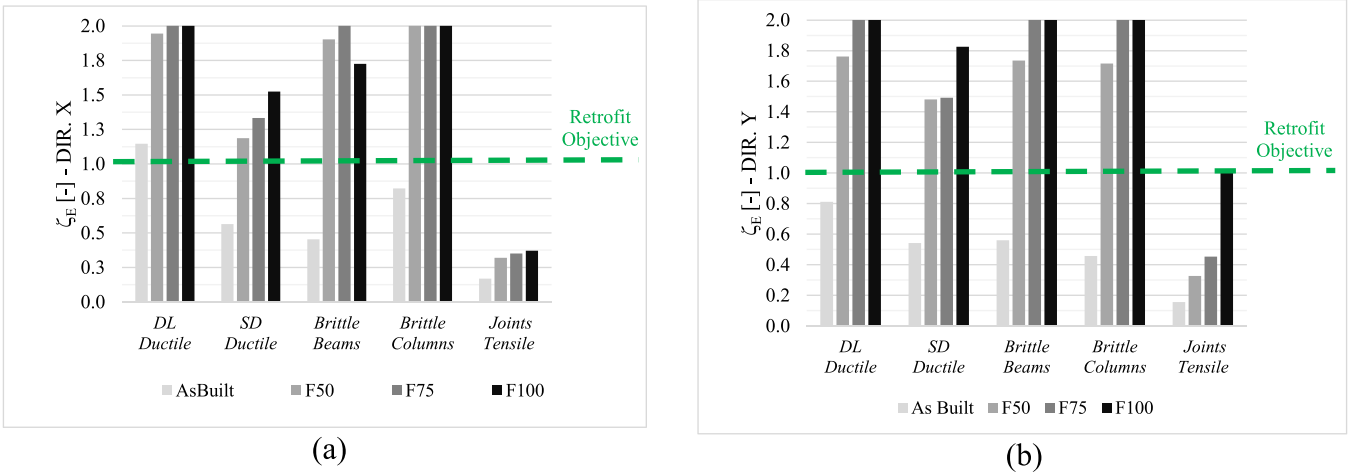


**Fig. 9.** Comparison in terms of safety index for ductile and brittle mechanisms along X (a) and Y (b).

interventions characterizing the three potential retrofit solutions explored in this study. As it could be expected, the initial intervention cost reduces with the decrease of the assumed design base shear force intensity. Such difference is mainly related to the gradual decrease of the intervention costs associated to the new steel exoskeleton and foundation upgrading, while the local intervention costs remained almost unchanged. In fact, the adoption of even the highest design force ("F100" scenario) was unable to reduce significantly the local failures and

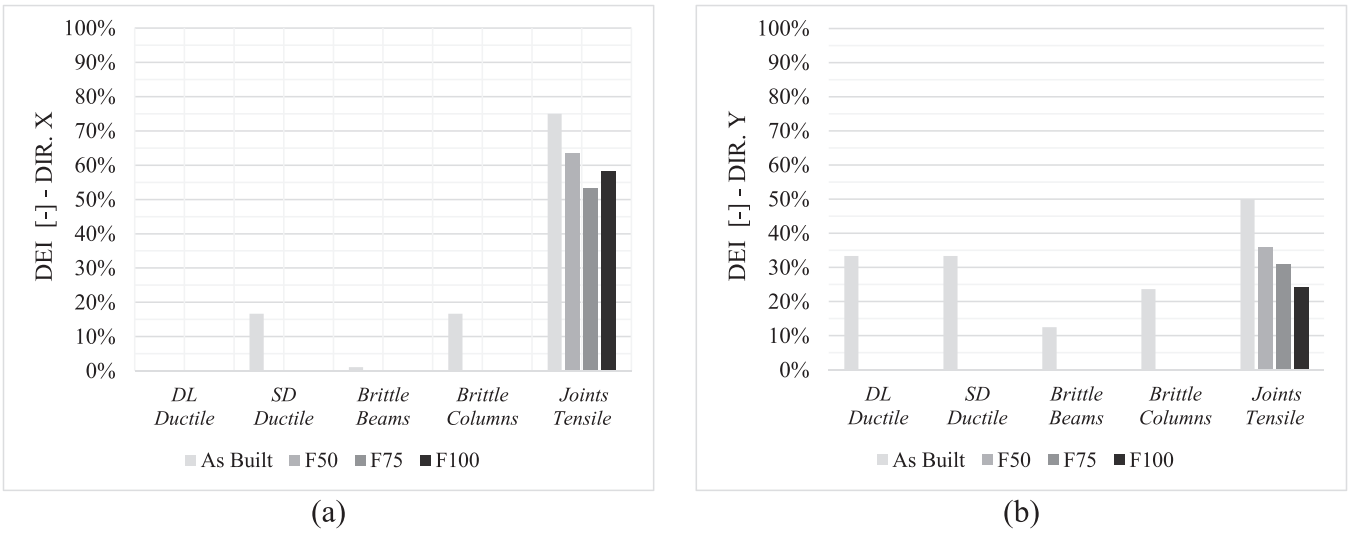


**Fig. 10.** Comparison in terms of DEI for ductile and brittle mechanisms along X (a) and Y (b).

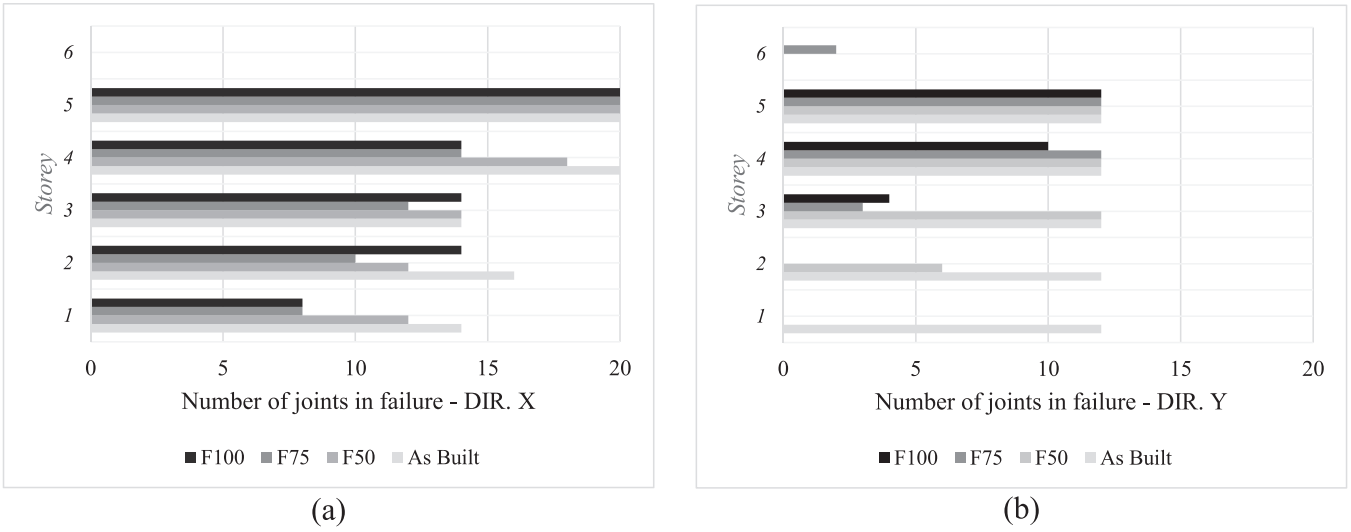


**Fig. 11.** Number and location of the failing RC beam-column joints, for a displacement demand corresponding to the SD limit state: X direction (a) and Y direction (b).

**Table 6**
Unit costs of interventions.

| *Intervention type* | Intervention | Unit cost |
|---|---|---|
| *Local* | External RC joint strengthening (FRP textile) | 3300 €/intervention |
| *Local* | Internal RC joint strengthening (RC jacketing) | 1500 €/intervention |
| *Global* | HE steel profiles (beams and columns) | 4.77 €/kg |
| *Global* | CHS steel profiles (braces) | 6.81 €/kg |
| *Global* | Connection system – F100 exoskeleton | 82.6 €/m |
| *Global* | Connection system – F75 exoskeleton | 71.6 €/m |
| *Global* | Connection system – F50 exoskeleton | 60.6 €/m |
| *Foundation* | Excavation, backfilling and concrete casting | 180 €/$m^3$ |
| *Foundation* | Self-drilling of micropiles, Diameter = 200 mm | 145.9 €/m |

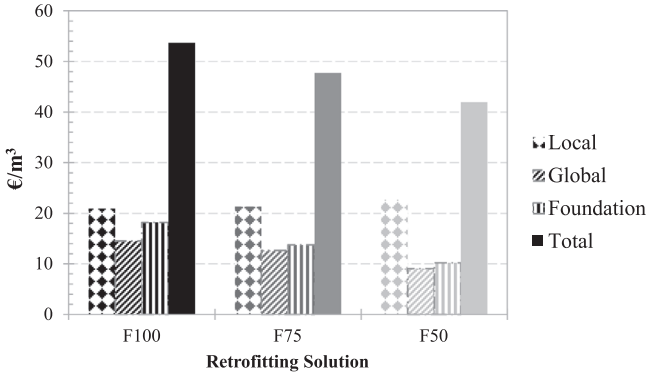


**Fig. 12.** Comparison among the upgrading solutions in terms of initial intervention cost per cubic meter of the existing structure.

damages (at beam-column joints), so that the costs related to the local interventions did not change. Though the costs of the new steel structure and relevant foundations can almost be halved by reducing the design force, the percentage decrease of the total costs when moving from the "F100" to the "F50" structure is only 22%, because of the local intervention costs remaining almost constant.

### 5.3. Preliminary cradle-to-gate life cycle assessment

In addition to the construction costs, it is of interest to examine the ecological footprint of any given intervention [50]. To ascertain which of the proposed design scenarios can effectively minimize the global warming potential (GWP), a widely accepted indicator of the environmental impact measured in kilograms of equivalent carbon dioxide ($kgCO_2$ eq.), the current study considered a "cradle-to-gate" assessment. The approach encompasses all the sub-processes involved in raw material extraction and manufacturing. The choice of this approach is motivated by the lack of unequivocal information regarding the successive phases, such as construction and end-of-life, which are necessary to perform the life cycle assessment (LCA) of each retrofit solution from a "cradle-to-grave" perspective.

The findings presented in this study are derived from pertinent research conducted on the materials utilized in structure-level interventions, such as concrete and steel [51,52], as well as the materials necessary for the member-level interventions, specifically the CFRP textiles [50,53]. The environmental impact of the self-drilling micro--piles, which were considered for the upgrading at the foundation level, was also included in this analysis, considering a typical Environmental Product Declaration of such elements [54]. This approach ensures that the obtained results reflect the significant variations in cradle-to-gate emissions that may arise when comparing the retrofit scenarios. It should be mentioned that the disruption of occupancy and the demolition of nonstructural components (which may have a slight influence on the comparison between the reported LCAs) were not considered due to the highly variable nature of their definition. Therefore, the considered average GWP values of the various interventions are reported in Table 7.

Fig. 13 reports a comparison in terms of GWP, highlighting the significant impact that structure-level techniques, based on the use of conventional materials of civil engineering (concrete and steel) have on the GWP estimation. Regarding the impact of the FRP textiles, although their production implies larger $CO_2$ emissions for each kg of product, their structural use results in relatively small quantities, thus making their "cradle-to-gate" carbon footprint almost irrelevant in comparison to more conventional materials [55–57].

Furthermore, it is noted that most of the GWP observed for the structure-level interventions is a direct consequence of the strengthening interventions considered at the foundation level, which implies large $CO_2$ emissions if compared to the CFRP textiles. However, one should also consider that concrete and, especially, steel are recyclable and/or reusable, which is an aspect not included in the GWP analysis presented herein. Therefore, further research is needed to improve the understanding of the overall environmental performance of structural materials throughout their entire life cycle.

## 6. Concluding remarks

The present study provides readers with a discussion about the multifaceted aspects implied by the decision-making process for seismic upgrading of existing RC frame structures that are not compliant to modern seismic codes.

Three force-based design criteria were adopted to design steel exoskeletons for seismic upgrading of an archetype 1960s RC frame structure. A first solution was based on designing a steel exoskeleton resisting the entire seismic force (a solution named "F100") i.e., completely neglecting any contribution from the existing RC frame structure. As alternatives, two additional steel exoskeletons were designed by considering reduced seismic shear forces equal to either 50% ("F50") or 75% ("F75") of the value adopted for the first case.

Correspondingly, nonlinear models were built for the existing RC frame and the new steel exoskeletons. The nonlinear models were submitted to pushover analysis and, both construction and ecologic costs were estimated along with a structural performance assessment.

The analysis results suggest that the modification of the global structural behaviour, obtained with the new steel exoskeletons, generally reduced the number of RC components failing in a brittle mode. However, such failures were not completely removed, even in the case of the "F100" design scenario i.e., the case of maximum value for the design shear force of the steel exoskeleton. Consequently, and based on the construction and ecologic cost benefits, it is advisable to design the steel exoskeleton with a reduced seismic force (as in the "F50" case), combining this intervention with a proper number of local RC strengthening techniques. With this approach, one can also reduce any upgrading interventions needed at the foundation level, thus gaining a considerable reduction of the economic and cradle-to-gate environmental impact of the whole retrofit system. Eventually, it is worth highlighting that the location of the brittle failures in the existing RC frame structure changed when comparing the bare existing RC frame with the hybrid RC-steel structural system. This implies the need for an analysis of the hybrid RC-steel structure response also to decide about any local strengthening of the existing RC frame.

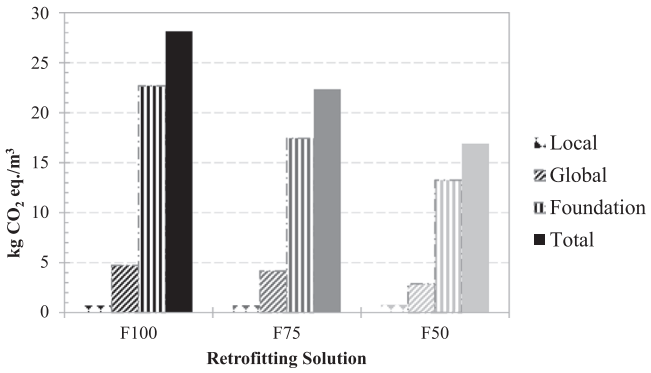


**Fig. 13.** Comparison among the upgrading solutions in terms of Global Warming Potential (GWP) per cubic meter of the existing structure.

**Table 7**
Unit Global Warming Potential (GWP) of interventions.

| *Intervention type* | Intervention | Unit cost |
|---|---|---|
| *Local* | External RC Joint strengthening (FRP textile) | 35 $kgCO_2$ eq./$m^2$ |
| *Local* | Internal RC Joint strengthening (RC jacketing) | 65 $kgCO_2$ eq./ intervention |
| *Global* | HE steel profiles (beams and column) | 2 $kgCO_2$ eq./kg |
| *Global* | CHS steel profiles (braces) | 2 $kgCO_2$ eq./kg |
| *Foundation* | Excavation and backfilling | 72 $kgCO_2$ eq./$m^3$ |
| *Foundation* | Concrete casting | 300 $kgCO_2$ eq./$m^3$ |
| *Foundation* | Self-drilling micropiles, Diameter = 200 mm | 2190 $kgCO_2$ eq./m |

## CRediT authorship contribution statement

**Nigro Francesco:** Writing – original draft, Visualization, Validation, Software, Investigation, Formal analysis, Data curation. **Martinelli Enzo:** Writing – review & editing, Supervision, Methodology, Formal analysis, Conceptualization. **Della Corte Gaetano:** Writing – review & editing, Supervision, Methodology, Formal analysis, Conceptualization.

## Declaration of Competing Interest

- All authors have participated in (a) conception and design, or analysis and interpretation of the data; (b) drafting the article or revising it critically for important intellectual content; and (c) approval of the final version.
- This manuscript has not been submitted to, nor is under review at, another journal or other publishing venue.

- The authors have no affiliation with any organization with a direct or indirect financial interest in the subject matter discussed in the manuscript

## Data availability

Data will be made available on request.

## Acknowledgements

This study is part of the ReLUIS-DPC 2022–2024 Project, funded by the Italian Civil Protection Department, whose financial contribution is gratefully acknowledged.

## References

[1] European Commission. EU Buildings Factsheets 2013. Available online: https://ec.europa.eu/energy/eu-buildings-factsheets_en (accessed on 1 October 2022).
[2] CNI, 2012. Elaboration of National Council of Engineers (CNI) Study Center on ISTAT, CRESME, and Civil Protection data, in Italian.
[3] Fardis MN, Abrams DP, Alcocer SM, Badoux M, Calvi MG, Carvalho EC, Elnashai AS, García LE, Kappos AJ, Kolias B, Kowalsky MJ, Machida A, Maffei J, Manfredi G, Moehle JP, Monti G, Nuti C, Otani S, Pantazopoulou SJ, Park R, Pinto PE, Priestley NM, Sucuoğlu H, Triantafillou TC. *fib* Bull 24 Seism Assess Retrofit Reinf Concr Build 2003. https://www.fib-international.org/publications/fib-bulletins/seismic-assessment-and-retrofit-of-reinforced-concrete-buildings-detail.html.
[4] Pan KY, Wu AC, Tsai KC, Li CH, Khoo HH. Seismic retrofit of reinforced concrete frames using buckling-restrained braces with bearing block load transfer mechanism. 0098-8847 Earthq Eng Struct Dyn 2016;45(14). https://doi.org/10.1002/eqe.2763.
[5] Cantisani G., Rodontini E., Della Corte G., (2021) Numerical modelling and analysis of eccentric bracing with vertical shear links. Eccomas Proceedia COMPDYN, 8th ECCOMAS Thematic Conference on Computational Methods in Structural Dynamics and Earthquake Engineering, 151–163, Streamed from Athens, Greece, 28 - 30 June 2021. DOI: 10.7712/120121.8470.19269.
[6] Della Corte G, Cantisani G. FEM Analysis of Steel Eccentric Braces for Seismic Retrofitting. Procedia Structural Integrity XIX ANIDIS Conference, Seismic Engineering in Italy 2023;44:472–9. https://doi.org/10.1016/j.prostr.2023.01.062.
[7] Della Corte G, D'Aniello M, Landolfo R. Field testing of all-steel buckling-restrained braces applied to a damaged reinforced concrete building. J Struct Eng 2015;141:0733–9445. https://doi.org/10.1061/(ASCE)ST.1943-541X.000108.
[8] Sutcu F, Bal A, Fujishita K, Matsui R, Celik OC, Takeuchi T. Experimental and analytical studies of sub-standard RC frames retrofitted with buckling-restrained braces and steel frames. Bull Earthq Eng 2020;18:2389–410. https://doi.org/10.1007/s10518-020-00785-4.
[9] Mazzolani FM, Della Corte G, D'Aniello M. Experimental analysis of steel dissipative bracing systems for seismic upgrading. J Civ Eng Manag 2009;15(1):7–19. https://doi.org/10.3846/1392-3730.2009.15.7-19.
[10] Mazzolani FM, Della Corte G, Cantisani G. Seismic Upgrading of an Existing Steel Structure Using Inverted Y-braces. Lecture Notes in Civil Engineering, Vol. 262. International Conference on the Behaviour of Steel Structures in Seismic Areas,; 2023. p. 890–7. https://doi.org/10.1007/978-3-031-03811-2_98.
[11] Scuderi G. Building exoskeletons for the integrated retrofit of social housing. Civ Eng J 2016;2:226–43. https://doi.org/10.28991/cej-2016-00000029.
[12] Marini A, Passoni C, Belleri A, Feroldi F, Preti M, Metelli G, Riva P, Giuriani E, Plizzari G. Combining seismic retrofit with energy refurbishment for the sustainable renovation of RC buildings: a proof of concept. Eur J Environ Civ Eng 2022;26(7):2475–95. https://doi.org/10.1080/19648189.2017.1363665.
[13] Marini A, Passoni C, Riva P, Negro P, Romano E, Taucer F. Technology options for earthquake resistant, eco-efficient buildings in Europe: Research needs. Report EUR 26497 EN. JRC87425. Luxembourg: Publications Office of the European Union; 2014. https://doi.org/10.2788/68902.
[14] Martelli L, Restuccia L, Ferro GA. The exoskeleton: a solution for seismic retrofitting of existing buildings. Procedia Struct Integr 2020;25:294–304. https://doi.org/10.1016/j.prostr.2020.04.034.
[15] Meglio E, Longobardi G, Formisano A. Integrated seismic-energy retrofit systems for preventing failure of a historical RC school building: comparison among metal lightweight exoskeleton solutions. Eng Fail Anal 2023;154:107663. https://doi.org/10.1016/j.engfailanal.2023.107663.
[16] Formisano A, Massimilla A, Di Lorenzo G, Landolfo R. Seismic retrofit of gravity load designed RC buildings using external steel concentric bracing systems. 1350-6307 Eng Fail Anal 2020;111:104485. https://doi.org/10.1016/j.engfailanal.2020.104485.
[17] Caterino N, Iervolino I, Manfredi G, Cosenza E. Comparative analysis of multi-criteria decision-making methods for seismic structural retrofitting. Comput-Aided Civ Infrastruct Eng 2009;24:432–45. https://doi.org/10.1111/j.1467-8667.2009.00599.x.
[18] Falcone R, Carrabs F, Cerulli R, Lima C, Martinelli E. Seismic retrofitting of existing RC buildings: a rational selection procedure based on Genetic Algorithms. Structures 2020;22:310–26. https://doi.org/10.1016/j.istruc.2019.08.006.
[19] Faella C., Martinelli E., Nigro E., (2008). A rational strategy for seismic retrofitting of RC existing buildings, The 14th World Conference on Earthquake Engineering October 12–17, 2008, Beijing, China.
[20] Balázs G.L., Cox B.N., Fardis M.N., Forbes J.M., Jirsa J.O., Kumar V., Monti G., Ozaka Y., Shehata L.D., Siviero E. & Walraven J.C. (2006), fib Bulletin 35, Retrofitting of concrete structures by externally bonded FRPs with emphasis on seismic applications.
[21] CNR-DT 200 R1/2013 (2013). Istruzioni per la progettazione, l'esecuzione ed il controllo di interventi di consolidamento statico mediante l'utilizzo di compositi fibrorinforzati.
[22] Corte Della, Barecchia G, Mazzolani F.M E. Seismic upgrading of RC buildings by FRP: Full-scale tests of a real structure. J Mater Civ Eng 2006;18(5):659–69. https://doi.org/10.1061/(ASCE)0899-1561(2006)18:5(659).
[23] Moshiri N, Martinelli E, Breveglieri M, Czaderski C. Experimental tests and numerical simulations on the mechanical response of RC slabs externally strengthened by passive and prestressed FRP strips. Eng Struct 2023;292:116559. https://doi.org/10.1016/j.engstruct.2023.116559.
[24] Nakashima M., Huang T., Lu L.W., (1983), Effects of diaphragm flexibility on seismic response of buildings structures. National Science Foundation Washington D. C. 20550. Fritz Laboratory Reports, Paper 2195.
[25] Sadashiva VK, MacRae GA, Deam BL, Spooner MS. Quantifying the seismic response of structures with flexible diaphragms. Earthq Eng Struct Dyn 2012;41:1365–89. https://doi.org/10.1002/eqe.1187.
[26] Lehman DE, Roeder CW, Herman D, Johnson S, Kotulka B. Improved seismic performance of gusset plate connections. J Struct Eng 2008;134(6):890–901. https://doi.org/10.1061/(ASCE)0733-9445(2008)134:6(890).
[27] Freeman SA, Nicoletti JP, Tyrell JV. Evaluations of existing buildings for seismic risk – a case study of Puget sound naval shipyard, Bremerton, Washington. Proceedings of U.S. national conference on earthquake engineering, Berkeley (USA). 1975.
[28] Veletsos A.S., Newmark N.M. (1960) Effect of inelastic behaviour on the response of simple systems to earthquake motions. In: Proceedings of the 2nd world conference on earthquake engineering, Tokyo, Japan, vol. 2. p. 895–912.
[29] Fajfar P. Capacity spectrum method based on inelastic demand spectra. Earthq Eng Struct Dyn 1999;28:979–93.
[30] Krawinkler H, Seneviratna GDPK. Pros and cons of a pushover analysis of seismic performance evaluation. Eng Struct 1997;Vol. 20:452–64. https://doi.org/10.1016/S0141-0296(97)00092-8.
[31] DM 17/01/2018. Italian Technical Code of Constructions; *Ministerial Decree*: Rome, Italy, 2018.
[32] EN 1998-1 (2005), Eurocode 8. Design of structures for earthquake resistance - Part 1: General rules, seismic actions and rules for buildings, European Committee for Standardization, Bruxelles.
[33] ANSI/AISC 341-22. Seismic Provisions for Structural Steel Buildings. An American National Standard 2022. https://www.aisc.org/globalassets/aisc/publications/standards/seismic-provisions-for-structural-steel-buildings-ansi-aisc-341-16.pdf.
[34] Reza Bayat M, Goel SC, Chao SH. Performance-based plastic design of earthquake resistant concentrically braced steel frames. Ann Arbor, MI: University of Michigan College of Engineering; 2010. 48109-2125. Available online at, ⟨https://www.aisc.org/globalassets/aisc/research-library/performance-based-plastic-design.pdf⟩.
[35] Sabelli R., (2000) Research on Improving the Design and Analysis of Earthquake Resistant Steel Braced Frames, FEMA/EERI Report, Washington, D. C. Available online at: https://citeseerx.ist.psu.edu/document?repid=rep1&type=pdf&doi=5ea4dcd27146422a0969b4e64422b73a479ced7b.
[36] Montuori R, Nastri E, Piluso V, Todisco P. Performance-based rules for the simplified assessment of steel CBFs. J Constr Steel Res 2022;191:107167. https://doi.org/10.1016/j.jcsr.2022.107167.
[37] Hung CC, Hsiao HJ, Shao Y, Yen CH. A comparative study on the seismic performance of RC beam-column joints retrofitted by ECC, FRP, and concrete jacketing methods. J Build Eng 2023;64:105691. https://doi.org/10.1016/j.jobe.2022.105691.
[38] Dhakal R. & Pan T. & Tsai K.C. (2003) Enhancement of Beam-Column Joint by RC Jacketing. Available online at: https://www.researchgate.net/publication/45448827_Enhancement_of_Beam-Column_Joint_by_RC_Jacketing.
[39] Bustamante, M., and Doix B. (1985) "Une méthode pour le calcul des tirants et des micropieux injectés", Bull. Liaison Lab. Ponts et Chaussées, Paris, n. 140, Ref. 3047, pp 75–92.
[40] EN 1997–1-1 (2004), Eurocode 7, Design of steel structures Part 1–1: Geotechnical design General rules, European Committee for Standardization, Bruxelles.
[41] Mazzoni S, McKenna F, Scott MH, Fenves GL, et al. OpenSees– Open System for Earthquake Engineering Simulation. Pacific Earthquake Engineering Research Center. Berkeley (USA): University of California; 2007. https://opensees.berkeley.edu/.
[42] EN 1993-1-1 (2005), Eurocode 3, Design of steel structures Part 1–1: General rules and rules for buildings, European Committee for Standardization, Bruxelles.
[43] Hsiao PC, Lehman DE, Roeder CW. A model to simulate special concentrically braced frames beyond brace fracture. Earthq Eng Struct Dyn 2013;42:183–200. ⟨http://doi.wiley.com/10.1002/eqe.2202⟩.
[44] Hsiao PC, Lehman DE, Roeder CW. Improved analytical model for special concentrically braced frames. J Constr Steel Res 2012;73:80–94. https://doi.org/10.1016/j.jcsr.2012.01.010.

[45] EN 1998–3, (2005), Eurocode 8. Design of Structures for Earthquake Resistance - Part 3: Assessment and Retrofitting of buildings, European Committee for Standardization, Bruxelles.
[46] C 21/01/2019, n. 7C.S.LL.PP. Instruction for the application of the DM 17/01/2018, Chapter 8, Ministerial Decree, Rome, Italy.
[47] EN 1992-1-1 (2005), Eurocode 2 - Design of concrete structures - Part 1–1: General rules and rules for buildings, European Committee for Standardization, Bruxelles.
[48] Regio Decreto 16/11/1939 n.2229, (1939), Rules for the execution of works in simple and reinforced concrete, Royal decree, Rome, Italy.
[49] Prezzario Campania LL.PP, (2022), Regional Price List of Public Works. Resolution of the Regional Council n.333 in 28/06/2022.
[50] Mistretta F, Stochino F, Sassu M. Structural and thermal retrofitting of masonry walls: An integrated cost-analysis approach for the Italian context. Build Environ 2019;155:127–36. https://doi.org/10.1016/j.buildenv.2019.03.033.
[51] Hart J, D'Amico B, Pomponi F. Whole-life embodied carbon in multistory buildings: steel, concrete and timber structures. J Ind Ecol 2021;25:403–18. https://doi.org/10.1111/jiec.13139.
[52] Tait M, Cheung W. A comparative cradle-to-gate life cycle assessment of three concrete mix designs. Int J Life Cycle Assess 2016;21:847–60. https://doi.org/10.1007/s11367-016-1045-5.
[53] Hohmann A., (2018), Life Cycle Assessment of Manufacturing Processes for CFRP Structures to Identify Optimization Potentials - Systematic Methodology for Estimating the Environmental Impact of Manufacturing Process Chains". Technical University of Munich. ⟨http://mediatum.ub.tum.de/1451614⟩.
[54] Minova SDA system for self-drilling micropiles, soil nails & rock bolts, (2021), Environmental Product Declaration Type III No. 140/2020. Available online at: https://geomek.se/wp-content/uploads/2021/04/MINOVA_EPD.pdf.
[55] Stoiber N, Hammerl M, Kromoser B. Cradle-to-gate life cycle assessment of CFRP reinforcement for concrete structures: calculation basis and exemplary application. J Clean Prod 2020;280:124300. https://doi.org/10.1016/j.jclepro.2020.124300.
[56] Das S. Life cycle assessment of carbon fiber-reinforced polymer composites. Int J Life Cycle Assess 2011;16:268–82. https://doi.org/10.1007/s11367-011-0264-z.
[57] Backes JG, Suer J, Pauliks N, Neugebauer S, Traverso M. Life cycle assessment of an integrated steel mill using primary manufacturing data: actual environmental profile. Sustainability 2021;13:3443. https://doi.org/10.3390/su13063443.